Accepted Manuscript

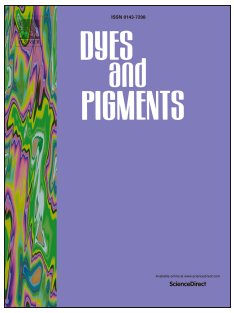

A reaction-based turn-on fluorescent sensor for the detection of Cu (II) with excellent sensitivity and selectivity: Synthesis, DFT calculations, kinetics and application in real water samples

Ming Tian, Huan He, Bei-Bei Wang, Xi Wang, Yi Liu, Feng-Lei Jiang

PII: S0143-7208(18)32723-2

DOI: https://doi.org/10.1016/j.dyepig.2019.02.043

Reference: DYPI 7377

To appear in: *Dyes and Pigments*

Received Date: 14 December 2018

Revised Date: 21 February 2019

Accepted Date: 24 February 2019

Please cite this article as: Tian M, He H, Wang B-B, Wang X, Liu Y, Jiang F-L, A reaction-based turn-on fluorescent sensor for the detection of Cu (II) with excellent sensitivity and selectivity: Synthesis, DFT calculations, kinetics and application in real water samples, *Dyes and Pigments* (2019), doi: https://doi.org/10.1016/j.dyepig.2019.02.043.

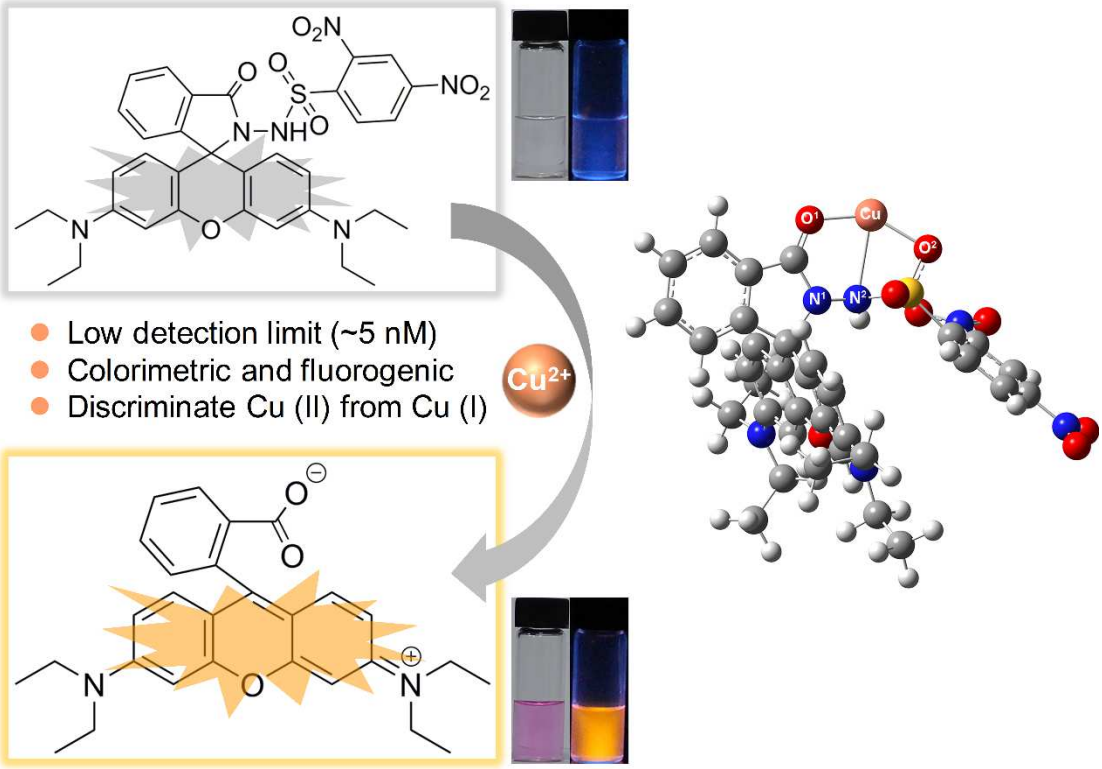

A Reaction-based Turn-on Fluorescent Sensor for the Detection of Cu (II) with Excellent Sensitivity and Selectivity: Synthesis, DFT Calculations, Kinetics and Application in Real Water Samples

Ming Tian [a], Huan He [a], Bei-Bei Wang [a], Xi Wang, Yi Liu [a,b,c] and Feng-Lei Jiang [a,*]

[a] State Key Laboratory of Virology & Key Laboratory of Analytical Chemistry for Biology and Medicine (Ministry of Education), College of Chemistry and Molecular Sciences, Wuhan University, Wuhan 430072, P. R. China

[b] School of Chemistry and Chemical Engineering, Wuhan University of Science and Technology, Wuhan 430081, P. R. China

[c] College of Chemistry and Materials Science, Nanning Normal University, Nanning 530001, P. R. China

*Corresponding Author. E-mail: fljiang@whu.edu.cn. Tel: +86-27-68756667.

Abstract:

A reaction-based turn-on fluorescent chemosensor **RhB-Cu**, starting from rhodamine B (**RhB**), for Cu^{2+} was easily synthesized in two steps. The sensor could selectively detect Cu^{2+} with a 100-fold fluorescence enhancement among the common metal ions, exhibiting an extremely low detection limit of 4.7 nM. To the best of our knowledge, this was the best record for the detection of Cu^{2+} with organic fluorescent sensors. There was a 1:1 binding stoichiometry between **RhB-Cu** and Cu^{2+} with an association constant of 6.42×10^4 M^{-1}. Noteworthy, it could distinguish Cu^{2+} from Cu^{+}, which was hard to realize in the previous studies. In addition, the detection mechanism was proposed based on mass spectrometric analysis and density functional theory (DFT) calculations. Kinetic studies were conducted to obtain the activation energy, enthalpy and entropy, so as to elucidate the solvent effect. Interestingly, the kinetic compensation effect (KCE) was uncovered in this work. Finally, **RhB-Cu** was proved to have the capability to work in real water samples. It would highly contribute to the even better design of fluorescent sensor for Cu^{2+} in future.

Keywords: fluorescent sensor, copper, PET mechanism, density functional theory (DFT), solvent effect, kinetic compensation effect (KCE)

1. Introduction

Copper, the third most abundant transition metal in the body [1], not only is the static metabolic cofactor at the center of enzymatic activity, but also can serve as dynamic signal that binds and regulates protein function at external allosteric sites [2,3]. Interestingly, copper is recently found to play a crucial role in neural activity toward a chemistry of consciousness [4]. Moreover, diseases such as Alzheimer's disease [5-7], Parkinson's disease [8,9], Menkes [10-12], Wilson disease [13,14], Huntington's [15], prion [17], obesity and diabetes [18,19] are suggested to be related to abnormal levels of copper ions. The limit of copper in drinking water, 1.3 ppm (~20 μM), is set by the US Environmental Protection Agency (EPA), and the average concentration of blood copper in the normal group is 15.7-23.6 μM [20] and of brain copper is ~ 0.1 mM [21]. Therefore, an efficient method for the detection of copper ions is full of significance. Traditional methods, including atomic absorption spectrometry (AAS) [22,23], surface plasmon resonance spectroscopy (SPR) [24], inductively coupled plasma atomic emission spectrometry (ICP-AES) [25], chromatography [26], voltammetry [27] and so on, have advantage of considerable sensitivity but shortcoming of time-consuming and complicated protocols. Thus, fluorescent chemosensors have been emerging for detection and are widely studied due to their simple instrumentation, good reproducibility, easy operation as well as better sensitivity [28-30].

In recent years, rhodamine, a well-known fluorophore, exhibits excellent photophysical properties as an ideal candidate for the design of fluorescent sensors [31-33], which include long-wavelength emission, large molar extinction-coefficient and high quantum yield. Most sensors based on rhodamine framework have successfully detected copper ion by utilizing the property of spirocyclic closed (non-fluorescent) and ring-opened (fluorescent) forms, which exhibits a "turn-on" signal response [34-37]. Nevertheless, there are few studies involved in chemical information about the mechanism, reaction kinetics and solvent effect.

Therefore, bearing these facts in mind, we designed and synthesized a

chemodosimeter **RhB-Cu**, in which Rhodamine B (**RhB**) as the fluorophore responded to Cu^{2+} based on the "turn-on" mechanism. The target product was easily prepared *via* a two-step procedure (Scheme 1). First, **RhB-1a** was prepared by the reaction of Rhodamine B with hydrazine hydrate. It had no fluorescence indicating its spirocycle form due to the quenching mechanism of photo-induced electron transfer (PET). Second, **RhB-Cu** was subsequently synthesized by reacting **RhB-1a** with 2,4-dinitrobenzenesulfonyl chloride (DNBS), a well-known fluorescence quencher. Consequently, the introduction of DNBS would further quench the fluorescence of **RhB**, which led to extremely low background and thereafter very high fluorescence turn-on ratio. Both **RhB-1a** and **RhB-Cu** were fully characterized by NMR and mass spectrometry (see the Supporting Information, Fig. S1-S6).

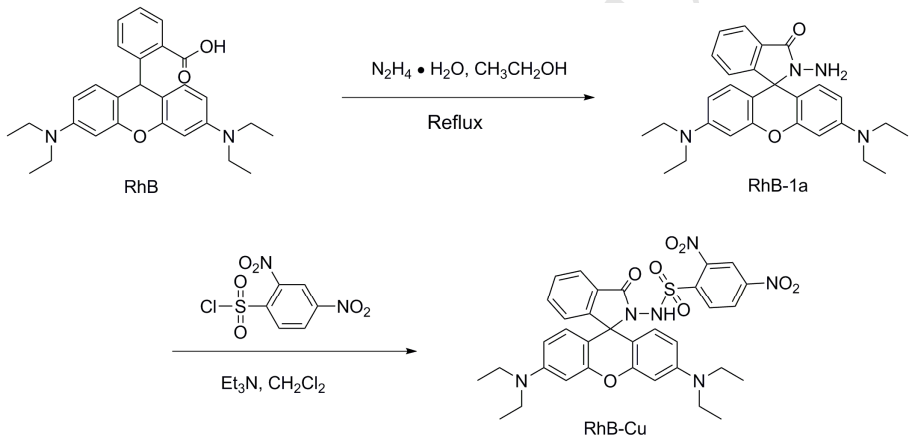

Scheme 1. Synthetic route of **RhB-Cu**.

2. Materials and methods

2.1. Chemicals and instrumentation

All regents and chemicals, unless otherwise stated, were used without further purification from the commercial resources. All glassware was oven-dried before used. NMR spectra were recorded on a Bruker AVANCE III HD 400 MHz spectrometer, using tetramethylsilane (TMS) as the internal standard. Mass spectra were measured with the Finnigan LCQ advantage mass spectrometer and the Agilent Technologies 6530 Q-TOF LC/MS. Fluorescent spectra were measured using a Perkin-Elmer LS-55 fluorescence spectrometer. A Cary 100 spectrophotometer was used to measure

absorption spectra. Fluorescent lifetimes were measured with a FLS1000 fluorescence spectrometer. Melt points were measured using a SGW X-4 Micromelting Point Apparatus.

2.2. Computational methods

The ground-state structures of the **RhB-Cu** and complexes based on **RhB-Cu** were optimized using the TD-DFT and DFT methods with the hybrid-generalized gradient approximation (HGGA) functional B3LYP. The 6-31g(d) basis set and the effective core potential LanL2DZ basis sets were respectively assigned to nonmetal elements (C, H, O, N and S) and metal elements [38]. A polarized continumm model (PCM) method was employed to treat the solvent effects of water and acetonitrile. All the calculations were performed with the Gaussian09 program package.

2.3. Preparation for solutions

The stock solution of **RhB-Cu** was prepared at 2 mM in dimethyl sulfoxide (DMSO). Testing solutions were prepared by diluting 4 μL of stock solution into 2 mL CH_3CN/H_2O (1:1, *v/v*) solution. Stock solutions (0.05 M, 4 μL) of metal ions including Ni^{2+}, Co^{2+}, Ca^{2+}, Li^{+}, Mg^{2+}, Zn^{2+}, Pb^{2+}, Cd^{2+}, Ag^{+}, Hg^{2+}, Fe^{3+}, Al^{3+}, Fe^{2+}, Mn^{2+}, Cr^{3+} and Cu^{+} were respectively added into the testing solutions. According to the previous report [39], stock solution for Cu^{+} was prepared by dissolving $Cu(MeCN)_4PF_6$ in CH_3CN under nitrogen conditions, while other metal ion stock solutions were derived from chloride salts. The fluorescence spectra were measured after the addition of each analytes.

3. Results and discussion

3.1. Computational study

The DFT calculations were performed for predicting the selectivity of **RhB-Cu** by calculating the energy of **RhB-Cu** and several representative complexes **RhB-Cu**-M (M: Cu^{2+}, Cu^{+}, Pb^{2+}, Al^{3+} and Hg^{2+}). It is found, except for Cu^{2+} and Cu^{+}, no converged complex between **RhB-Cu** and Pb^{2+}, Al^{3+} or Hg^{2+} could be obtained, indicating that potential complexes of **RhB-Cu**-Pb^{2+}, **RhB-Cu**-Al^{3+} and

RhB-Cu-Hg^{2+} may not exist. However, **RhB-Cu** and **RhB-Cu**-Cu^{+} are speculated non-fluorescent due to the PET mechanism, which is explained by the molecular orbitals calculated from TD-DFT. Four molecular orbitals (from HOMO to HOMO-2, LUMO+2) of **RhB-Cu** are mainly located at the **RhB** moiety, while another two molecular orbitals (LUMO and LUMO+1) are mainly located at the DNBS group. Thus, after the electron is excited from HOMO, HOMO-1 or HOMO-2 to the LUMO+2 orbital of **RhB** group, the electron may be transferred to LUMO+1 or LUMO orbital due to the fact that the energy of LUMO (LUMO+2 orbital of the whole molecule) of **RhB** moiety is higher than the LUMO (LUMO orbital of the whole molecule) of the DNBS moiety (Fig. 1a). As a result, the electron of higher electron state could be transferred to the lowest vibrational state which provides the non-emissive path for electron transition [38]. However, when **RhB-Cu** is complexed with Cu^{2+}, on the contrary, the HOMO and LUMO orbitals of **RhB-Cu**-Cu^{2+} are mainly distributed on **RhB** moiety, while the LUMO+1 and LUMO+2 orbitals are distributed on the DNBS moiety (Fig. 1b). When the electron is excited from HOMO to the LUMO orbital of **RhB** moiety, it goes back directly accompanied by fluorescence, owing to the fact that the unoccupied molecular orbitals with DNBS character are higher in energy than the LUMO with **RhB** character. In another word, the PET process is blocked and the fluorescence is recovered. Moreover, when **RhB-Cu** is complexed with Cu^{+}, the mechanism of the fluorescence quenching by Cu^{+} is similar to the **RhB-Cu** due to a similar distribution of molecular orbitals to **RhB-Cu** (Fig. 1c). It is worth noting that the transitions of electrons in molecular orbitals under excitation mentioned here all have a large oscillator strength (Table S1).

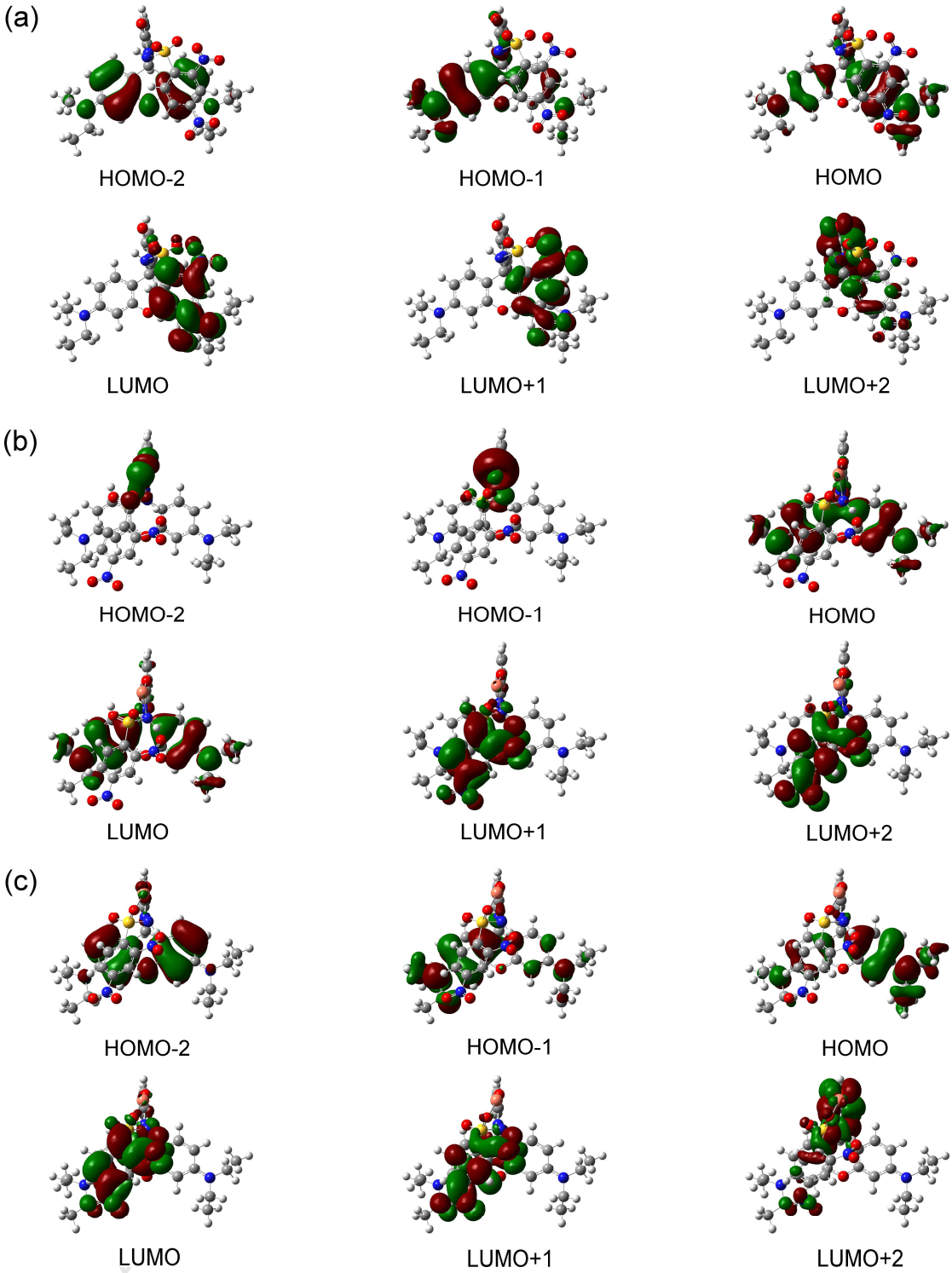

Fig. 1. Molecular orbitals calculated at B3LYP/6-31g(d)/LANL2DZ level for (a) **RhB-Cu**, (b) **RhB-Cu**-Cu^{2+} and (c) **RhB-Cu**-Cu^{+}.

3.2. Selective reaction of RhB-Cu with Cu^{2+} and possible sensing mechanism

The fluorescence spectra further suggest that **RhB-Cu** can distinguish Cu^{2+} from

other metal ions, including Ni^{2+}, Co^{2+}, Ca^{2+}, Li^{+}, Mg^{2+}, Zn^{2+}, Pb^{2+}, Cd^{2+}, Ag^{+}, Hg^{2+}, Fe^{3+}, Al^{3+}, Fe^{2+}, Mn^{2+}, Cr^{3+} and Cu^{+}. Obviously, only Cu^{2+} leads to a 100-fold fluorescence enhancement due to the turn-on mechanism with ring-opening of **RhB-Cu** induced by Cu^{2+} (Fig. 2a-c), which is in perfect agreement with the above theoretical calculations. Visually, only Cu^{2+} can trigger the occurrence of distinct pink color and orange fluorescence (Fig. 2e). Moreover, different types of anions including Cl^{-}, SO_4^{2-}, CH_3COO^{-}, NO_3^{-} and Br^{-} don't affect the fluorescence intensity of the **RhB-Cu** in response to Cu^{2+} (Fig. S7). A coordination reaction with the 1:1 binding stoichiometry between **RhB-Cu** and Cu^{2+} is confirmed by the Job's plot (Fig. 2d). Besides, a peak at *m/z* 443.3 in the mass spectrum corresponds to **RhB** and a peak at *m/z* 749.9 corresponds to the complex of **RhB-Cu** with Cu^{2+} (Fig. S8). Moreover, the results of HPLC-MS showed that the retention times of **RhB-Cu** and **RhB** were 0.696 min and 0.513 min, and their corresponding molecular weights were 687.2231 and 443.2232, respectively, while the retention time and corresponding molecular weight were 0.520 min and 443.2333 after the reaction of **RhB-Cu** with 25 equiv. of Cu^{2+}, which also indicated the formation of **RhB** (Fig. S9-S11). Furthermore, DFT was performed for calculating the bonding length of **RhB-Cu**-Cu^{2+}, which implied that N^1 is too far away from the copper atom to form a coordination bond (Table 1). Therefore, a possible sensing mechanism can be proposed as follows. The coordination reaction with the 1:1 binding stoichiometry may proceed firstly by means of a copper atom coordinating with N^2, O^1 and O^2 atoms of **RhB-Cu**, which promotes the PET and subsequently causes the ring opening of the **RhB-Cu** accompanied by fluorescence enhancement (Fig. 3).

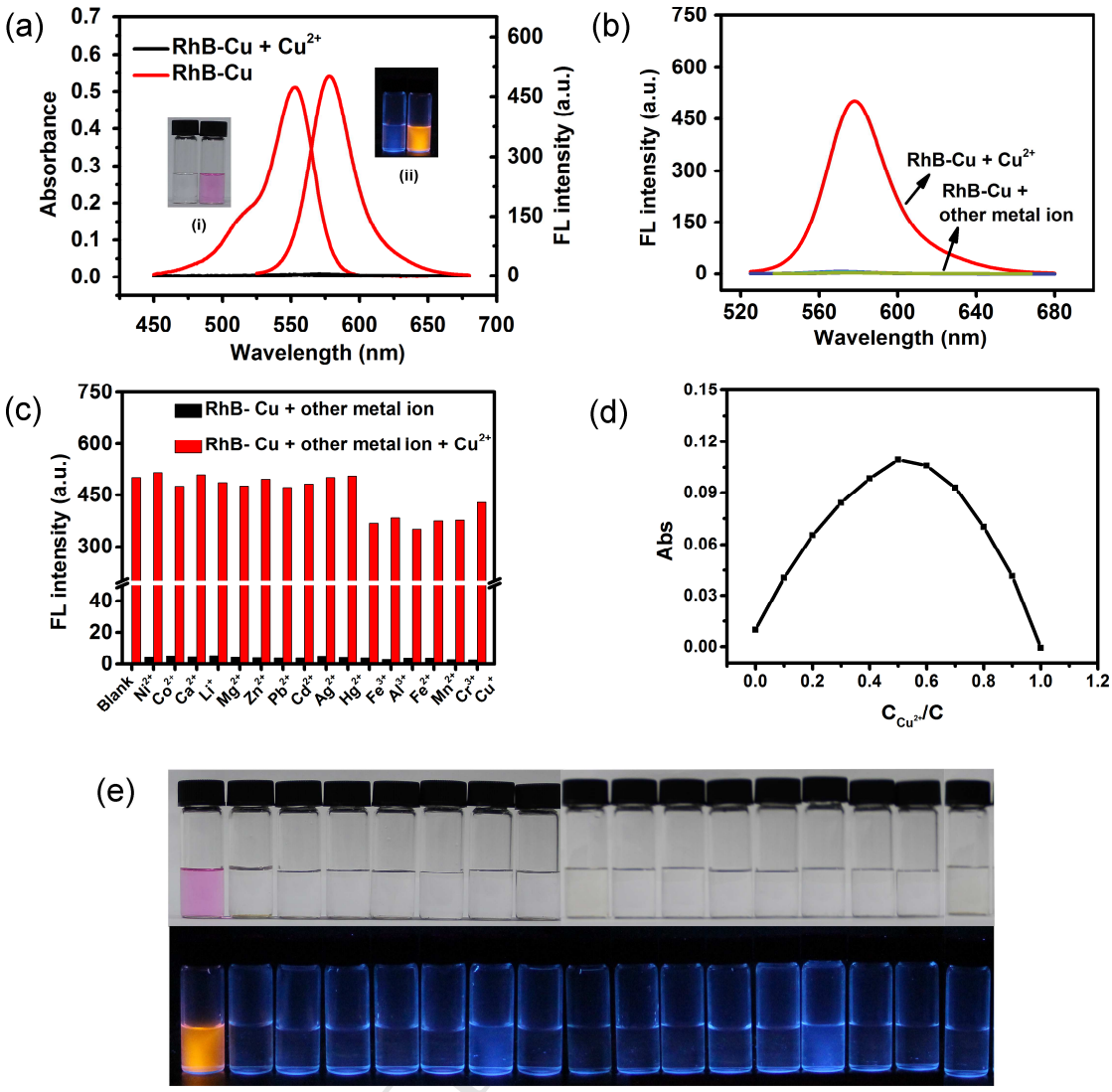

Fig. 2. (a) UV-vis and fluorescence spectra of **RhB-Cu** (4 μM) in the absence and presence of 25 equiv. of Cu^{2+} in CH_3CN/H_2O (1:1, *v/v*) solution. The insets show the photo of **RhB-Cu** (left) and **RhB-Cu** in the presence of Cu^{2+} (right) under ambient (i) and UV light (ii), respectively. (b) Fluorescence spectra of **RhB-Cu** (4 μM, λ_{ex} = 500 nm) exposed to 25 equiv. of Cu^{2+} and other metal ions in CH_3CN/H_2O (1:1, *v/v*) solution at room temperature. Other metal ions: blank, Ni^{2+}, Co^{2+}, Ca^{2+}, Li^{+}, Mg^{2+}, Zn^{2+}, Pb^{2+}, Cd^{2+}, Ag^{+}, Hg^{2+}, Fe^{3+}, Al^{3+}, Fe^{2+}, Mn^{2+}, Cr^{3+} and Cu^{+} ions. (c) The black bar is the histogram of (b), the red bar is the fluorescence response of the sensor with Cu^{2+} (25 equiv.) and different analytes. (d) Job's plot according to the method for continuous variations. The total concentration of **RhB-Cu** and Cu^{2+} is 10 μM in

CH_3CN/H_2O (1:1, *v/v*) solution. (e) Photos of **RhB-Cu** with different metal ions under ambient light (top) and UV irradiation at 365 nm (bottom). From left to right: Cu^{2+}, Fe^{3+}, Ni^{2+}, Co^{2+}, Ca^{2+}, Li^{+}, Mg^{2+}, Al^{3+}, Fe^{2+}, Zn^{2+}, Mn^{2+}, Cr^{3+}, Pb^{2+}, Cd^{2+}, Hg^{2+}, Ag^{+}, Cu^{+}.

Table 1 The distances between Cu atom and coordination atoms of **RhB-Cu**-Cu^{2+} performed by DFT.

Atom-atom	Bond distance (Å)
Cu-O^1	1.84424
Cu-N^1	2.95103
Cu-N^2	2.49361
Cu-O^2	1.92089

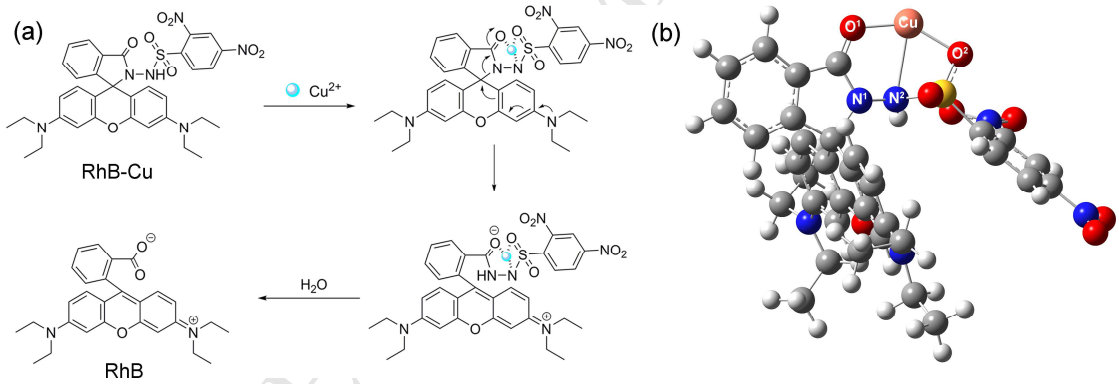

Fig. 3. (a) Proposed mechanism for the reaction of **RhB-Cu** with Cu^{2+}. (b) The optimized structure of **RhB-Cu**-Cu^{2+} by DFT.

3.3. Fluorescence titration with Cu^{2+} and pH effects

More attractively, after titration of various amounts of Cu^{2+}, the detection limit of **RhB-Cu** for sensing Cu^{2+} was found to be as low as 4.7 nM with a signal-to-noise ratio of 3 (Fig. 4a and b). Compared with the performances of the recently reported sensors for Cu^{2+} (Table 2), the **RhB-Cu** herein not only has an extremely low

detection limit for Cu^{2+} but also can effectively distinguish Cu^{2+} from Cu^{+}, indicating the excellent sensitivity and selectivity of the **RhB-Cu**. Moreover, after addition of Cu^{2+}, the solution of **RhB-Cu** changed from colorless to pink immediately and the complete enhancement of the fluorescence intensity occurred within 5 min at 25 ºC. This response time is quite competitive.

According to previous studies [40,41], modified Benesi-Hildebrand expression has been given as:

$$\frac{F_{\max} - F_0}{F - F_0} = 1 + \frac{1}{K[M]^n} \qquad (1)$$

where F_0, F and $F_{\max}$ are the fluorescence intensities of **RhB-Cu** in the absence of Cu^{2+}, in the presence of different concentrations of Cu^{2+} and for complete reaction, respectively, K is the binding constant, $[M]$ is the concentration of Cu^{2+} and n is the number of Cu^{2+} bound per **RhB-Cu**.

The linear relationship between $1 / (F - F_0)$ and $1 / [M]$ confirms the 1:1 stoichiometry for binding of Cu^{2+} by **RhB-Cu** with an association constant of 6.42×10^4 M^{-1} (Fig. 4c). Otherwise, the pH effect on the detection capability suggests that the **RhB-Cu** is stable in the pH range from 4 to 8 (Fig. 4d).

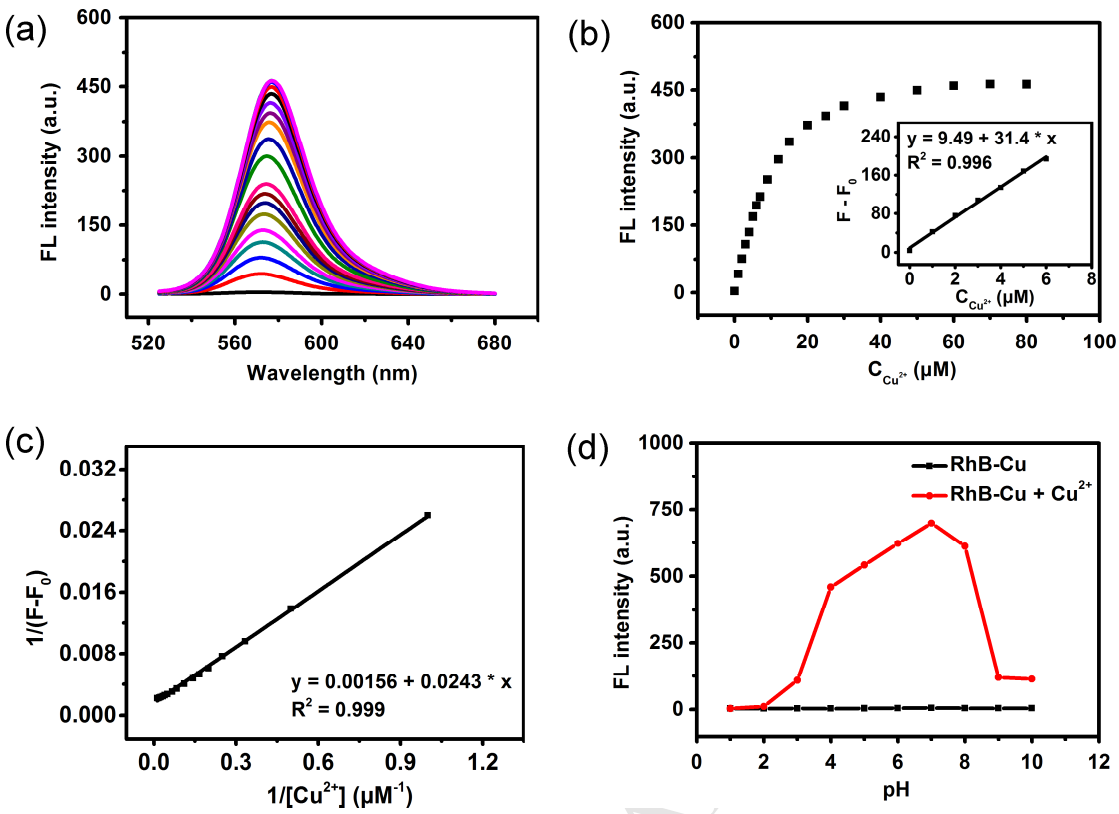

Fig. 4. (a) Fluorescence spectra of **RhB-Cu** (4 μM) with increasing concentration of Cu^{2+} (0 - 20 equiv.) in CH_3CN/H_2O (1:1, *v/v*) solution (λ_{ex} = 500 nm, λ_{em} = 580 nm). (b) The plot of the fluorescence intensity of **RhB-Cu** titrated with increasing concentrations of Cu^{2+} at 580 nm. The inset shows the linear range of the curve. (c) Benesi-Hildebrand plot for the reaction of **RhB-Cu** with Cu^{2+}. (d) Fluorescence intensity of **RhB-Cu** (4 μM) and **RhB-Cu** with 25 equiv. of Cu^{2+} at 580 nm under different pH conditions (λ_{ex} = 500 nm).

Table 2 The performances of the recently reported sensors for Cu^{2+}.

Sensor	Target	$\lambda_{ex}/\lambda_{em}$ (nm)	LOD (nM)	K_a (M^{-1})	Response to Cu^{+}	mechanism	Ref.
1	Cu^{2+}	745/770	50	2.70×10^6	NA	PET	[42]
2	Cu^{2+}	425/522	40	NA	No response	ICT	[43]
3	Cu^{2+}, Al^{3+}	520/555	9.9	1.10×10^6	NA	PET	[44]
4	Cu^{2+}	515/585	110	9.32×10^4	NA	PET	[45]
5	Cu^{2+}	520/617	310	NA	NA	NA	[46]
6	Cu^{2+}	380/570	42	NA	NA	FRET	[47]
7	Cu^{2+}	420/570	18.6	NA	NA	FRET	[48]
8	Cu^{2+}, Fe^{3+}	370/508	140	8.60×10^4	NA	NA	[49]
9	Cu^{2+}, Hg^{2+}	254/342	615	5.65×10^4	NA	PET	[50]
10	Cu^{2+}, Al^{3+}	470/530	677	3.94×10^7	NA	NA	[51]
RhB-Cu	Cu^{2+}	500/580	4.7	6.42×10^4	No response	PET	This work

LOD: Limit of detection. NA: Not available. K_a is association constant.

3.4. The reaction kinetics in solution

The physicochemical properties of solvent molecules should be considered to study the reaction kinetics in solutions, which could be affected by many factors including dielectric constant, polarity, ionic strength and solvation. On the other hand, the change of kinetic parameters in different solvents to some extent also reflects changes of the reaction itself. In this regard, DFT was performed to calculate the total energy of the reaction between **RhB-Cu** and Cu^{2+} in H_2O and CH_3CN, whose values were -2784341.40 and -2784354.16 kcal mol^{-1}, respectively, indicating that the energy barrier required for this reaction with CH_3CN as solvent was lower than that with H_2O as solvent. It should be noting that, the DFT calculation without considering entropy change would have deviation from the experimental results.

So, further investigation of **RhB-Cu** exposed to Cu^{2+} in a mixture solution with different ratios of CH_3CN and H_2O (*v/v*) was conducted (Fig. 5a-e). The rate constants could be obtained by fitting the fluorescence intensity (*F*) as a function of reaction

times (t) with a first order kinetic equation (2):

$$F = \mathrm{A}' + \mathrm{B}'\exp(-kt) \qquad (2)$$

where F is the fluorescence intensity, k is the pseudo-first-order kinetic rate constant, t is the reaction time, and A' and B' are constants. Then, the relationship between rate constant and temperature can be described by Arrhenius equation (3):

$$\ln k = \ln A - \frac{E_{\mathrm{a}}}{\mathrm{R}T} \qquad (3)$$

where A is the pre-exponential factor, E_{a} is the apparent activation energy, R is the gas constant (8.314 J mol^{-1} K^{-1}), and T is the absolute temperature. According to the Transition State Theory (TST), the enthalpy and entropy of activation are calculated to help elucidate the solvent effect. For the reaction in the condensed phase, standard molar enthalpy of activation ($\Delta_{\mathrm{r}}^{\neq} H_{\mathrm{m}}^{\Theta}$) could be obtained by the equation (4):

$$\Delta_{\mathrm{r}}^{\neq} H_{\mathrm{m}}^{\Theta} = E_a - RT \qquad (4)$$

Furthermore, according to the thermodynamic functions at the given temperature, standard molar entropy of activation ($\Delta_{\mathrm{r}}^{\neq} S_{\mathrm{m}}^{\Theta}$) could be obtained by the equation (5):

$$k = \frac{k_{\mathrm{B}}T}{h}(c^{\Theta})^{1-\mathrm{n}} \exp\left[\frac{\Delta_{\mathrm{r}}^{\neq} S_{\mathrm{m}}^{\Theta}(c^{\Theta})}{R}\right] \exp\left[-\frac{\Delta_{\mathrm{r}}^{\neq} H_{\mathrm{m}}^{\Theta}(c^{\Theta})}{RT}\right] \qquad (5)$$

where k_{B} is the Boltzmann constant (1.38 × 10^{-23} J K^{-1}), h is the Planck constant (6.626 × 10^{-34} J S^{-1}) and c^{Θ}= 1mol dm^{-3}.

Then, a series of kinetic parameters were obtained with different percentage of CH_3CN (20% ~ 50%) in H_2O (*v/v*) (Table 3). The activation entropy ($\Delta_{\mathrm{r}}^{\neq} S_{\mathrm{m}}^{\Theta}$) and activation energy (E_{a}) increase with the increasing percentage of CH_3CN in the mixed solvent indicating that the solvent effect really exists. Actually, in the mixed solvent system of CH_3CN and H_2O, the **RhB-Cu**, lower solubility in water, was surrounded by acetonitrile molecules, that is a form of solvation compound. When Cu^{2+} is added, solvent effect could be destroyed due to complexation. From this perspective, the higher percentage of CH_3CN in the mixed solvent, the more obvious the solvent effect and the more difficult the reaction between **RhB-Cu** and Cu^{2+}, which could lead to increased disorder, entropy, and energy barrier. The experimental results also showed $\Delta_{\mathrm{r}}^{\neq} H_{\mathrm{m}}^{\Theta} > 0$, demonstrating that the formation of transition state is endothermic. Taking

into account the $\Delta_r^{\neq}S_m^{\theta}$ and $\Delta_r^{\neq}H_m^{\theta}$, a conclusion could be drawn that as the CH_3CN content in the mixture solution increases, both the $\Delta_r^{\neq}S_m^{\theta}$ and $\Delta_r^{\neq}H_m^{\theta}$ will increase and the $\Delta_r^{\neq}S_m^{\theta}$ substantially increase, which suggests that the formation of transition state gradually changes from enthalpy driven to entropy driven due to the solvent effect.

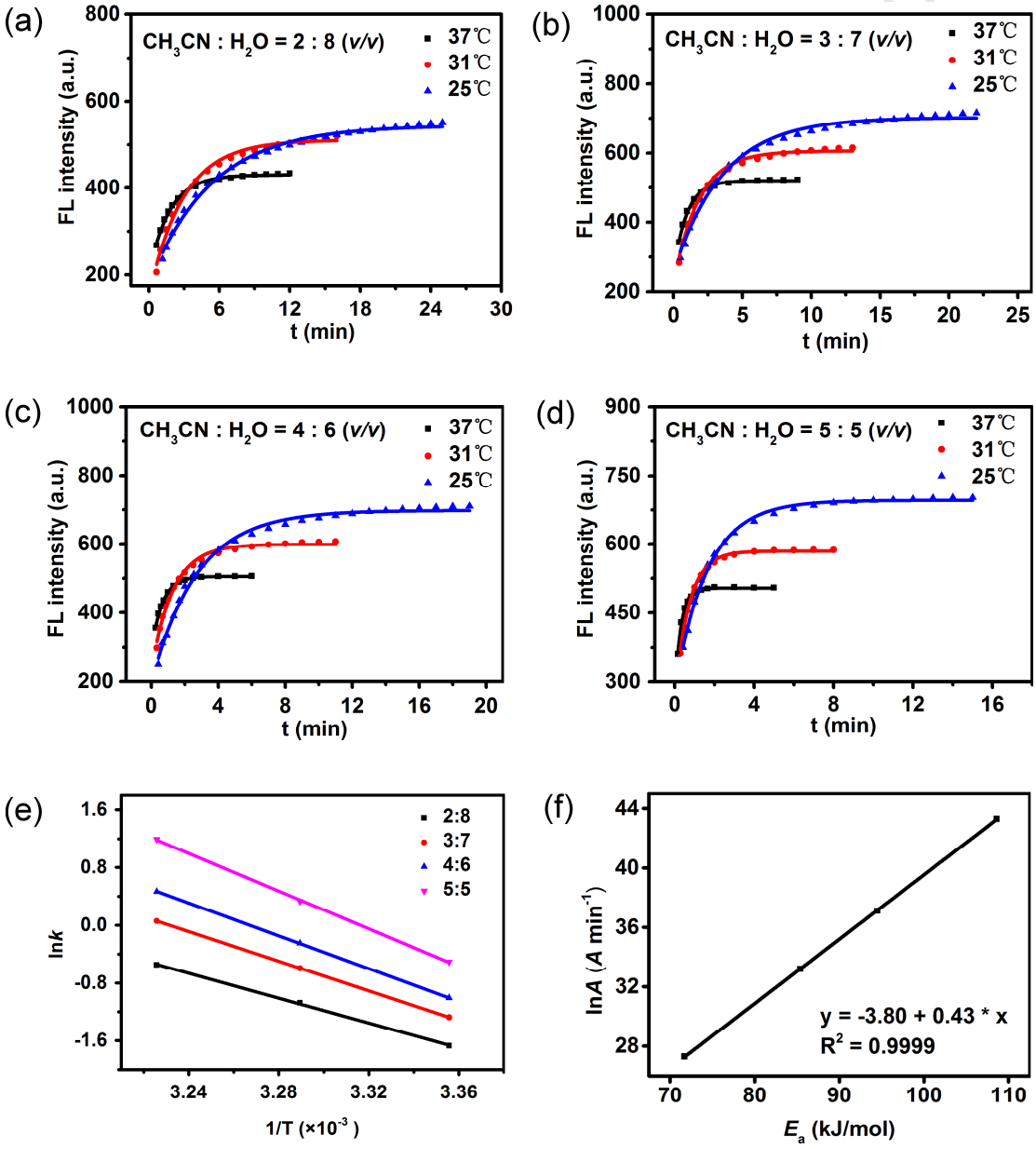

Fig. 5. First order kinetic fitting curves for the reaction of the **RhB-Cu** with Cu^{2+} at different ratio (*v/v*) of CH_3CN and H_2O mixture. (a) CH_3CN: H_2O, 2:8 (*v/v*), (b) CH_3CN: H_2O, 3:7 (*v/v*), (c) CH_3CN: H_2O, 4:6 (*v/v*), and (c) CH_3CN: H_2O, 5:5 (*v/v*). (e)

The effect of temperature on the rate constant according to Arrhenius equation, where k is rate constant and T is temperature. (f) The relationship between ln A and E_a.

Table 3 Kinetic parameters obtained from the pseudo-first-order at different ratio of CH_3CN and H_2O (*v/v*) mixture.

CH_3CN : H_2O (*v/v*)	k (min^{-1}) 310 K	304 K	298 K	R^2	E_a ($kJ\cdot mol^{-1}$)	ln$A$ (min^{-1})	$\Delta_r^{\neq} H_m^{\theta}$ ($kJ\cdot mol^{-1}$)	$\Delta_r^{\neq} S_m^{\theta}$ ($kJ\cdot mol^{-1}\cdot K^{-1}$)
2:8	0.5766	0.3405	0.1881	0.9989	71.7	27.3	69.2	-60.5
3:7	1.0606	0.5506	0.2794	0.9999	85.4	33.2	82.9	-11.4
4:6	1.5954	0.7776	0.3645	0.9999	94.5	37.1	92.0	21.5
5:5	3.2853	1.3945	0.6022	0.9994	108.6	43.3	106.1	72.8

3.5. The kinetic compensation effect (KCE)

Interestingly, the logarithm of preexponential factor A has a positive linear correlation with the E_a indicating that the kinetic compensation effect (KCE) possibly exist in the reaction system (Fig. 5f). According to previous reports [52,53], the pre-exponential factor A and the activation energy E_a often obey the following relationship:

$$\ln A = a \times E_a + b \qquad (6)$$

Where a and b are constants for a series of related process. This relationship is referred to as the kinetic compensation effect (KCE), which means that according to Arrhenius eq. (3), an increase of activation energy will not result in a decrease of the reaction rate due to a compensatory increase of A. Basically, KCE is accompanied by the appearance of isokinetic point (T_{iso}, ln k_{iso}), which in turn verifies the validity of the kinetic compensation effect. According to eq. (6), ln k_{iso} could be calculated by eq. (7):

$$\ln k_{iso} = b \qquad (7)$$

Further, T_{iso} can be calculated by eq. (8):

$$T_{\mathrm{iso}} = \frac{1}{R \times a} \qquad (8)$$

Besides, ln k_{iso} could also be calculated by eq. (3) at T_{iso}. In this work, the mean value of $(\ln k)|_{T=T_{\mathrm{iso}}}$ is -3.49, which is very close to -3.80 as indicated in the compensation plot (Fig. 5f). This result confirms the KCE obtained in the reactions of **RhB-Cu** with Cu^{2+} at different percentage of CH_3CN (20% ~ 50%) in H_2O.

3.6. Calculation of PL decay parameters

Moreover, the radiative and nonradiative rates of **RhB-Cu** in the presence of Cu^{2+} were obtained according to the following equations [54]:

$$k_{\mathrm{r}} = \frac{\Phi}{\tau} \qquad (9)$$

$$k_{\mathrm{nr}} = \frac{1-\Phi}{\tau} \qquad (10)$$

where k_{r} and k_{nr} are the radiative and nonradiative rates, respectively, and Φ is the relative quantum yield and τ is the average lifetime. Φ, τ, k_{r} and k_{nr} for the reaction of the **RhB-Cu** with Cu^{2+} have little change at different ratio (*v/v*) of CH_3CN and H_2O (Table 4), which suggests that the change of solvent has little effect on the ring opening of **RhB-Cu** and fluorescence emission.

Table 4 Relative quantum yields, lifetimes, radiative rates and nonradiative rates for the reaction of the **RhB-Cu** and Cu^{2+} at different ratio (*v/v*) of CH_3CN and H_2O.

CH_3CN: H_2O (*v/v*)	Φ	R^2	τ (ns)	χ^2	k_{r} (10^8 s^{-1})	k_{nr} (10^8 s^{-1})
1:9	--	--	1.87 ± 0.00289	0.951	--	--
2:8	0.504	0.9988	1.97 ± 0.00297	0.935	2.56	2.52
3:7	0.498	0.9989	1.97 ± 0.00295	0.898	2.53	2.55
4:6	0.503	0.9993	1.98 ± 0.00297	0.912	2.54	2.51
5:5	0.493	0.9974	2.03 ± 0.00299	0.952	2.43	2.50

3.7. Application of RhB-Cu for the detection of Cu^{2+} in water samples

With the above results in hand, we applied **RhB-Cu** for Cu^{2+} detection in real water samples. Under the optimized conditions, East Lake (in Wuhan city, Hubei

province, P. R. China) water samples were analyzed by the proposed fluorescence spectroscopic method. The recovery rates of Cu^{2+} in the lake water are in the range of 108.4% - 113.5% (Table 5), which indicates that the **RhB-Cu** could be used for the highly sensitive detection of Cu^{2+} in real water samples.

Table 5 Determination of Cu^{2+} in real water samples by **RhB-Cu**.

Samples	Added (μM)	Detected (mean ± SD, n = 4)	Recovery (%)
Lake Water	1.500	1.626 ± 0.067	108.4
	2.000	2.250 ± 0.078	112.5
	2.500	2.837 ± 0.045	113.5
	3.000	3.315 ± 0.081	110.5
	3.500	3.822 ± 0.078	109.2

4. Conclusion

In conclusion, a Rhodamine B-based turn-on fluorescent chemodosimeter (**RhB-Cu)** for Cu^{2+} was designed and synthesized with a facile method. This fluorescent sensor had an extremely low detection limit of 4.7 nM with a fast response time of 5 min. It could distinguish Cu^{2+} from other metal ions, including Ni^{2+}, Co^{2+}, Ca^{2+}, Li^{+}, Mg^{2+}, Zn^{2+}, Pb^{2+}, Cd^{2+}, Ag^{+}, Hg^{2+}, Fe^{3+}, Al^{3+}, Fe^{2+}, Mn^{2+}, Cr^{3+} and Cu^{+}, which was proved by fluorescence spectrometry and TD-DFT calculation. Moreover, a possible mechanism was proposed based on fluorescence spectroscopy, HPLC-MS and DFT calculations. The coordination reaction with the 1:1 binding stoichiometry may proceed firstly by means of a copper atom coordinating with N^2, O^1 and O^2 atoms of **RhB-Cu**, which promotes the PET and subsequently causes the ring opening of the **RhB-Cu** accompanied by fluorescence enhancement. In addition, a series of kinetic parameters for the reaction of the **RhB-Cu** with Cu^{2+} were obtained in the mixed solvent indicating that the solvent effect really exists. Furthermore, kinetic studies uncovered the kinetic compensation effect. Finally, **RhB-Cu** had good performances

in the detection of Cu^{2+} in real water samples. Future efforts should be devoted to further improvement of the specific response to copper ions by increasing the water solubility and reversibility of the sensor as well as the detection of endogenous copper ions in the organism.

Acknowledgments

The authors gratefully acknowledge the financial support from the National Natural Science Foundation of China (21573168, 21773178, 21873075), the Natural Science Foundation of Hubei Province (2018CFA090), Guangxi Science and Technology Project (GuiKeAD17195081), Bagui Scholar Program of Guangxi Province, the Fundamental Research Funds for the Central Universities (2042017kf0170) and Large-scale Instrument and Equipment Sharing Foundation of Wuhan University.

References

[1] G.T. Sfrazzetto, C. Satriano, G.A. Tomaselli, E. Rizzarelli, Synthetic fluorescent probes to map metallostasis and intracellular fate of zinc and copper, *Coord. Chem. Rev.* 311 (2016) 125-167.

[2] C.J. Chang, Searching for harmony in transition-metal signaling, *Nat. Chem. Biol.* 11 (2015) 744.

[3] A.T. Aron, K.M. Ramos-Torres, J.A. Cotruvo Jr, C.J. Chang, Recognition-and reactivity-based fluorescent probes for studying transition metal signaling in living systems, *Acc. Chem. Res.* 48 (2015) 2434-2442.

[4] C.J. Chang, Bioinorganic life and neural activity: toward a chemistry of consciousness? *Acc. Chem. Res.* 50 (2017) 535-538.

[5] P.S. Donnelly, Z. Xiao, A.G. Wedd, Copper and Alzheimer's disease, *Curr. Opin. Chem. Biol.* 11 (2007) 128-133.

[6] M.G. Savelieff, S. Lee, Y. Liu, M.H. Lim, Untangling amyloid-β, tau, and metals in Alzheimer's disease, *ACS Chem. Biol.* 8 (2013) 856-865.

[7] A. Pal, M. Siotto, R. Prasad, R. Squitti, Towards a unified vision of copper involvement in Alzheimer's disease: a review connecting basic, experimental, and clinical research, *J. Alzheimer's Dis.* 44 (2015) 343-354.

[8] C.G. Dudzik, E.D. Walter, G.L. Millhauser, Coordination features and affinity of the Cu^{2+} site in the α-synuclein protein of Parkinson's disease, *Biochemistry* 50 (2011) 1771-1777.

[9] E. Carboni, P. Lingor, Insights on the interaction of alpha-synuclein and metals in the pathophysiology of Parkinson's disease, *Metallomics* 7 (2015) 395-404.

[10] M. DiDonato, B. Sarkar, Copper transport and its alterations in Menkes and Wilson diseases, *Biochim. Biophys. Acta, Mol. Basis Dis.* 1360 (1997) 3-16.

[11] I.D. Goodyer, E.E. Jones, A.P. Monaco, M.J. Francis, Characterization of the Menkes protein copper-binding domains and their role in copper-induced protein relocalization, *Hum. Mol. Genet.* 8 (1999) 1473-1478.

[12] S.G. Kaler, ATP7A-related copper transport diseases-emerging concepts and future trends, *Nat. Rev. Neurol.* 7 (2011) 15.

[13] S. Lutsenko, Atp7b-/- mice as a model for studies of Wilson's disease, *Biochem. Soc. Trans.* 36 (2008) 1233–1238.

[14] M.L. Graper, D. Huster, S.G. Kaler, Lutsenko, S.; Schilsky, M. L.; Thiele, D. J. Introduction to human disorders of copper metabolism, *Ann. N. Y. Acad. Sci.* 1314 (2014) 37-44.

[15] G. Xiao, Q. Fan, Wang, X.; Zhou, B. Huntington disease arises from a combinatory toxicity of polyglutamine and copper binding, *Proc. Natl. Acad. Sci. U. S. A.* 110 (2013) 14995-15000.

[16] P. Davies, P.C. McHugh, V.J. Hammond, F. Marken, D.R. Brown, Contribution of individual histidines to prion protein copper binding. *Biochemistry* 50 (2011) 10781-10791.

[17] A.J. McDonald, J.P. Dibble, E.G. Evans, G.L. Millhauser, A new paradigm for enzymatic control of α-cleavage and β-cleavage of the prion protein, *J. Biol. Chem.* 289 (2014) 803–813.

[18] D. Huster, S. Lutsenko, Wilson disease: not just a copper disorder. Analysis of a Wilson disease model demonstrates the link between copper and lipid metabolism, *Mol. BioSyst.* 3 (2007) 816-824.

[19] T.E. Engle, Copper and lipid metabolism in beef cattle: A review, *J. Anim. Sci.* 89 (2011) 591-596.

[20] H.S. Jung, P.S. Kwon, J.W. Lee, J.I. Kim, C.S. Hong, J.W. Kim, S. Yan, J.Y. Lee, J.H. Lee, T. Joo, J.S. Kim, Coumarin-derived Cu^{2+}-selective fluorescence sensor: synthesis, mechanisms, and applications in living cells, *J. Am. Chem. Soc.* 131 (2009) 2008-2012.

[21] J.R. Prohaska, Functions of trace elements in brain metabolism, *Physiol. Rev.* 67 (1987) 858-901.

[22] M. Soylak, I. Narin, M. Dogan, Trace enrichment and atomic absorption spectrometric determination of lead, copper, cadmium and nickel in drinking water samples by use of an activated carbon column, *Anal. Lett.* 30 (1997) 2801-2810.

[23] M. Ghaedi, F. Ahmadi, A. Shokrollahi, Simultaneous preconcentration and determination of copper, nickel, cobalt and lead ions content by flame atomic absorption spectrometry, *J. Hazard. Mater.* 142 (2007) 272-278.

[24] E.S. Forzani, H. Zhang, W. Chen, N. Tao, Detection of heavy metal ions in drinking water using a high-resolution differential surface plasmon resonance sensor, *Environ. Sci. Technol*. 39 (2005) 1257-1262.

[25] Y. Liu, P. Liang, L. Guo, Nanometer titanium dioxide immobilized on silica gel as sorbent for preconcentration of metal ions prior to their determination by inductively coupled plasma atomic emission spectrometry, *Talanta*. 68 (2005) 25-30.

[26] A. Ali, H. Shen, X. Yin, Simultaneous determination of trace amounts of nickel, copper and mercury by liquid chromatography coupled with flow-injection on-line derivatization and preconcentration, *Anal. Chim. Acta.* 369 (1998) 215-223.

[27] A. Bobrowski, K. Nowak, J. Zarębski, Application of a bismuth film electrode to the voltammetric determination of trace iron using a Fe (III)-TEA-BrO_3-catalytic system, *Anal. Bioanal. Chem.* 382 (2005) 1691-1697.

[28] Y. Zhao, Y. Ren, H. Li, T. Han, H. Chen, W. Guo, A new far-red naphthorhodamine dye: Synthesis, fluorescent probe and bioimaging applications, *Dyes Pigments* 132 (2016) 255-261.

[29] X. Gu, Q. Chen, Z. Fang, A novel fluorescent probe based on β-C-glycoside for quantification of bovine serum albumin, *Dyes Pigments* 139 (2017) 334-343.

[30] F. Xu, W. Tang, S. Kang, J. Song, X. Duan, A highly sensitive and photo-stable fluorescent probe for endogenous intracellular H_2O_2 imaging in live cancer cells, *Dyes Pigments* 153 (2018) 61-66.

[31] J. Liu, Y. Qian, A novel naphthalimide-rhodamine dye: intramolecular fluorescence resonance energy transfer and ratiometric chemodosimeter for Hg^{2+} and Fe^{3+}, *Dyes Pigments* 136 (2017) 782-790.

[32] M. Hong, S. Lu, F. Lv, D. Xu, A novel facilely prepared rhodamine-based Hg^{2+} fluorescent probe with three thiourea receptors, *Dyes Pigments* 127 (2016) 94-99.

[33] A.A. Soares-Paulino, L. Giroldo, G. Celante, C. Lodeiro, A.A. Dos Santos, Formation of an emissive telluroxide promoted by Hg^{2+} in aqueous environment: A new naked-eye and ratiometric rhodamine dimer fluorescent Mercury (II) probe, *Dyes Pigments* 159 (2018) 121- 127.

[34] V. Dujols, F. Ford, A.W. Czarnik, A long-wavelength fluorescent chemodosimeter selective for Cu (II) ion in water. *J. Am. Chem. Soc.* 119 (1997) 7386-7387.

[35] X. Chen, T. Pradhan, F. Wang, J.S. Kim, J. Yoon, Fluorescent chemosensors based on spiroring-opening of xanthenes and related derivatives. *Chem. Rev.* 112 (2011) 1910-1956.

[36] S. Pu, L. Ma, G. Liu, H. Ding, B. Chen, A multiple switching diarylethene with a phenyl-linked rhodamine B unit and its application as chemosensor for Cu^{2+}. *Dyes Pigments* 113 (2015) 70-77.

[37] H. Kang, C. Fan, H. Xu, G. Liu, S. Pu, A highly selective fluorescence switch for Cu^{2+} and Fe^{3+} based on a new diarylethene with a triazole-linked rhodamine 6G unit. *Tetrahedron* 74 (2018) 4390-4399.

[38] T. Rasheed, C. Li, Y. Zhang, F. Nabeel, J. Peng, J. Qi, L. Gong, C. Yu, Rhodamine-based multianalyte colorimetric probe with potentialities as on-site assay kit and in biological systems. *Sens. Actuators, B* 258 (2018) 115-124.

[39] S.C. Dodani, A. Firl, J. Chan, C.I. Nam, A.T. Aron, C.S. Onak, K.M. Ramos-Torres, J. Paek, C.M. Webster, M.B. Feller, C.J. Chang, Copper is an endogenous modulator of neural circuit spontaneous activity. *Proc. Natl. Acad. Sci*. 111 (2014) 16280-16285.

[40] M. Barra, C. Bohne, J.C. Scaiano, Effect of cyclodextrin complexation on the photochemistry of xanthone. Absolute measurement of the kinetics for triplet-state exit, *J. Am. Chem. Soc*. 112 (1990) 8075-8079.

[41] M. Sohrabi, M. Amirnasr, H. Farrokhpour, S. Meghdadi, A single chemosensor with combined ionophore/fluorophore moieties acting as a fluorescent "Off-On" Zn^{2+} sensor and a colorimetric sensor for Cu^{2+}: Experimental, logic gate behavior and TD-DFT calculations, *Sens. Actuators, B* 250 (2017) 647-658.

[42] P. Li, X. Duan, Z. Chen, Y. Liu, T. Xie, L. Fang, X. Li, M. Yin, B.A Tang, near-infrared fluorescent probe for detecting Copper (II) with high selectivity and sensitivity and its biological imaging applications, *Chem. Commun.* 47 (2011) 7755-7757.

[43] M. Xu, C. Yin, F. Huo, Y. Zhang, J. Chao, A highly sensitive "ON-OFF-ON" fluorescent probe with three binding sites to sense copper ion and its application for cell imaging, *Sens. Actuators, B* 204 (2014) 18-23.

[44] V.K. Gupta, N. Mergu, L.K. Kumawat, A new multifunctional rhodamine-derived probe for colorimetric sensing of Cu (II) and Al (III) and fluorometric sensing of Fe (III) in aqueous media, *Sens. Actuators, B* 223 (2016) 101-113.

[45] B. Zhang, Q. Diao, P. Ma, X. Liu, D. Song, X. Wang, A sensitive fluorescent probe for Cu^{2+} based on rhodamine B derivatives and its application to drinking

water examination and living cells imaging, *Sens. Actuators, B* 225 (2016) 579-585.

[46] H. Ding, B. Li, S. Pu, G. Liu, D. Jia, Y. Zhou, A fluorescent sensor based on a diarylethene-rhodamine derivative for sequentially detecting Cu^{2+} and arginine and its application in keypad lock, *Sens. Actuators, B* 247 (2017) 26-35.

[47] Y. Ge, X. Zheng, R. Ji, S. Shen, X. Cao, A new pyrido [1,2-a] benzimidazole-rhodamine FRET system as an efficient ratiometric fluorescent probe for Cu^{2+} in living cells, *Anal. Chim. Acta.* 965 (2017) 103-110.

[48] J. Tang, S. Ma, D. Zhang, Y. Liu, Y. Zhao, Y. Ye, Highly sensitive and fast responsive ratiometric fluorescent probe for Cu^{2+} based on a naphthalimide-rhodamine dyad and its application in living cell imaging, *Sens. Actuators, B* 236 (2016) 109-115.

[49] B. Zhang, H. Liu, F. Wu, G. Hao, Y. Chen, C. Tan, Y. Tan, Y. Jiang, A dual-response quinoline-based fluorescent sensor for the detection of Copper (II) and Iron (III) ions in aqueous medium, *Sens. Actuators, B* 243 (2017) 765-774.

[50] J. Dong, Y. Liu, J. Hu, H. Baigude, H. Zhang, A novel ferrocenyl-based multichannel probe for colorimetric detection of Cu (II) and reversible fluorescent “turn-on” recognition of Hg (II) in aqueous environment and living cells, *Sens. Actuators, B* 255 (2018) 952-962.

[51] X. Zhang, P. Sun, F. Li, H. Li, H. Zhou, H. Wang, B. Zhang, Z. Pan, Y. Tian, X. Zhang, A tissue-permeable fluorescent probe for Al (III), Cu (II) imaging in vivo, *Sens. Actuators, B* 255 (2018) 366-373.

[52] N. Liu, R. Zong, L. Shu, J. Zhou, W. Fan, Kinetic compensation effect in thermal decomposition of cellulosic materials in air atmosphere. *J. Appl. Polym. Sci.* 89 (2003) 135-141.

[53] E.L. Mui, W.H. Cheung, V.K. Lee, G. McKay, Compensation effect during the pyrolysis of tyres and bamboo. *Waste Manage*. 30 (2010) 821-830.

[54] R. Prajapati, S. Chatterjee, A. Bhattacharya, T.K. Mukherjee, Surfactant-induced modulation of nanometal surface energy transfer from silicon quantum dots to silver nanoparticles, *J. Phys. Chem. C.* 119 (2015) 13325-13334.

Highlights:

- The probe **RhB-Cu** for Cu (II) had an extremely low detection limit of 4.7 nM.
- The probe **RhB-Cu** can distinguish Cu (II) from Cu (I).
- The kinetic compensation effect (KCE) was proved in this work.